Study on Energy of Formation of NiTi and NiZr intermetallic compounds using DFT

A dissertation submitted in partial fulfillment of the requirements
for the award of the degree
B. Tech in Metallurgical and Materials Engineering.
Submitted by:

Deepnika Jain
16MT12

Akhilesh Kamble
16MT19

Under the guidance of
Dr. B. Rajasekaran

Department of Metallurgical and Materials Engineering
National Institute of Technology, Karnatka

June 16, 2020

DECLARATION

by Deepnika Jain and Akhilesh Kamble

We hereby declare that the Project Work Report entitled **Study on Energy of Formation of NiTi and NiZr intermetallic compounds using DFT** which is being submitted to the **National Institute of Technology Karnataka, Surathkal** for the award of the Degree of Bachelor of Technology in **Metallurgical and Materials Engineering** is a *bonafide report* of the work carried out by us. The material contained in this Project Work Report has not been submitted to any University or Institution for the award of any degree.

Deepnika Jain
16MT12

Akhilesh Kamble
16MT19

Department of Metallurgical and Materials Engineering

Place: NITK, SURATHKAL
Date: June 16, 2020

CERTIFICATE

This is to *certify* that the B.Tech. Project Work Report entitled **Study on Energy of Formation of NiTi and NiZr intermetallic compounds using DFT** submitted by

16MT12

Deepnika Jain

16MT19

Akhilesh Kamble

as a record of the work carried out by them, is accepted as the *B.Tech. Project Work Report submission* in partial fulfillment of the requirements for the award of the degree of **Bachelor of Technology in Metallurgical and Materials Engineering**.

Guide: Dr. B. Rajasekaran

Chairman - DUGC

Abstract

Density Functional Theory (DFT) calculation is a powerful tool to understand ground state structure and properties of metals and alloys. The binary compounds NiTi and NiZr are in different crystal structure, even though they have many similarities like same ratio of elements, melt congruently and Ti and Zr are both in HCP crystal structure. In the present work, energy of formation of NiTi and NiZr system are calculated using Quantum Espresso software and compared with literature data. This methodology is helpful to determine the unstable and metastable structures which can be used in CALPHAD approach to determine the phase diagram of the Ni-Ti-Zr ternary alloy system.

Acknowledgements

It gives us immense pleasure to thank everyone who has helped us out at National Institute of Technology, Karnataka during our four memorable years. With great honor and respect, we thank our guide **Dr. B. Rajasekaran**, Department of Metallurgical and Materials Engineering, NITK, Surathkal, for guiding us throughout this work. We also thank him for providing and arranging the required facilities and timely suggestions. We will always be indebted to him for his kind support and guidance. We also received valuable suggestions throughout our experiments and also while writing this report from **Dr. K. Santhy**, Associate Professor at Institute of Technology and Engineering, Indus University, Ahmedabad. We would also like to thank our U.G. Project Examination committee members, **Dr. Jagannatha Nayak**, **Dr. Subray R. Hegde**, **Dr. Saumen Mandal** and **Dr. Sumanth Govindarajan** for their critical assessment during our presentation and valuable suggestions.

Contents

List of Tables

List of Figures

List of Codes

Chapter 1

Introduction

Shape Memory alloys (SMAs) are a unique class of alloys with varied engineering applications. They exhibit shape memory effect, superelasticity, damping capabilities, extraordinary fatigue resistance and hysteresis loop in stress-strain curve for loading, unloading and shape recovery process.

One of the most common SMA is Nickel-Titanium alloy called Nitinol (Nickel Titanium Naval Ordnance Laboratory). The story of Nitinol as an extraordinary material, its discovery in 1959 by William J. Buehler of the U.S. Naval Ordnance Laboratory and its subsequent development by Buehler and Frederick E. Wang has been well documented by [Kauffman and Mayo, 1997]. The alloy was widely used for orthopedic implants, cardiovascular surgery, orthodontics, solid-state heat engines, shock absorbers and for other applications that require properties of SMAs. Apart from shape memory effect and superelasticity, nitinol in particular exhibits high strength, good corrosion resistance, bio-compatibility, ductility, kink resistance and vibration and shock damping. It is also non-magnetic, thus enabling usage in MRI.

1.1 Motivation

Despite its revolution, the problem with nitinol was realized later, especially with medical implants. The problem with nickel is that the metal may leach out in the form of toxic Ni^{2+} ions. To increase the corrosion resistance of nitinol and to limit the release of Ni^{2+}

toxic ions, small amounts of zirconium i.e. 5-10 atomic percent are added into the existing nitinol system. The experimental results obtained by adding Zr to nitinol have been well documented by [Khan et al., 2017].

The addition of Zr has marked changes in the properties of nitinol. Ni-Ti has a single phase microstructure. With the addition of Zr, multiple phases are formed. The increase in Zr content in the alloy causes a change in its microstructure and hence in the electrode-electrolyte interface, which favors the formation of Zr oxides. This increased the corrosion resistance of the resulting alloys. Addition of Zr also lead to an increase in hardness values. The overall benefit of adding Zr to the alloy has inspired various studies including this.

1.2 Aims and Objectives

Subsequent research has been carried out to model the ternary system based on the required properties. Present work concentrates on determining the energy of formation of NiTi and NiZr using DFT method. The objective of the project is,

- To study the crystallographic information of NiTi and NiZr system.
- To optimize the cut-off energy and k-points for NiTi and NiZr system using single point energy calculation.
- To determine the ground state energy of Ni-FCC, Ti and Zr in HCP, NiTi-B2 and NiZr-orthorhombic crystal structure using geometric optimization.
- To determine the energy of formation of NiTi and NiZr and compare with literature data.

Chapter 2

Background and Related Work

2.1 Ab initio Thermodynamics

With the advancements in high performance computing, it is now possible to carry out intensive low length scale calculations for systems with large numbers of atoms and molecules. Amongst these calculations, total energy calculations based on Density Functional Theory (DFT) have gained much use in the context of CALPHAD. Results from these calculations often serve as input in the thermodynamic modelling, greatly improving the quality of the Gibbs energy functions. The predictive capability of DFT can be utilized to obtain the structural, electronic and thermodynamic properties of materials. Thermo-chemical properties such as enthalpy of formation, enthalpy of mixing, etc. serve as important input in the optimization of Gibbs energy functions. When the experimental values are unavailable, estimated values of these properties can be used in the optimization. Besides, the enthalpy of formation of several hypothetical end-members of the sublattice formulation may be required. These quantities can be obtained using ab initio calculations based on DFT. In the past, semi-empirical methods such as the Miedema model [Miedema, 1973] were used for estimating the enthalpy of formation. At present, methods based on DFT are being used for generating thermochemical information such as, enthalpy of formation and enthalpy of mixing at absolute temperature with good accuracy. A brief overview about this technique is given in the next section.

2.1.1 Density Functional Theory

The time-independent non-relativistic Schrödinger equation for a many-body system consisting of N nuclei and n electrons is given as,

$$\hat{H}\psi(R_I, r_i) = E\psi(R_I, r_i) \tag{2.1}$$

where, R_I is the co-ordinate of nucleus, r_i is the co-ordinate of electron, $\hat{H}$ is the Hamiltonian operator, E is the eigenvalue (total energy at 0 K) and $\psi(R_I, r_i)$ is the wave-function or eigenfunction representing the many-body wave-function.
The exact Hamiltonian for a many-body system is given as,

$$\hat{H} = -\frac{1}{2}\sum_{I}^{N}\frac{1}{M_I}\nabla_I^2 \; -\frac{1}{2}\sum_{i}^{n}\nabla_i^2 - \frac{1}{2}\sum_{I}^{N}\sum_{i}^{n}\frac{Z_I}{|r_i - R_I|} + \frac{1}{2}\sum_{i}^{n}\sum_{j\neq i}^{n}\frac{1}{|r_j - r_i|} + \frac{1}{2}\sum_{I}^{N}\sum_{J\neq I}^{N}\frac{Z_I Z_J}{|R_J - R_I|} \tag{2.2}$$

where M_I is the mass of the nucleus and Z_I is the valence charge of the nucleus. The first two terms of the Hamiltonian denotes the kinetic energy of nuclei and electrons, respectively. The third term corresponds to the coulombic attraction between electron and nucleus at coordinates i and I. The last two terms represent the coulombic repulsion between two electrons with coordinates i and j as well as two nuclei with coordinates I and J, respectively. The many-body Schrödinger equation with an exact Hamiltonian cannot be solved completely, except for hydrogen atoms. Though it is possible to solve the problem numerically, it will be very demanding even for a small system. As the computational time increases with increase in number of particles in the system, it is imperative to adopt a few approximations to speed up the calculations.

2.1.2 Born-Oppenheimer approximation

The easiest approximation that can be employed is the Born-Oppenheimer or adiabatic approximation [Born, 1927]. It is based on the fact that nucleus is much heavier ($m_p \approx 1800\ m_e$) than electrons and nuclear motion is three orders of magnitude slower than

motion of electrons. Hence, it can be assumed that the nuclei are stationary with respect to the electrons. Based on this approximation, Equation (2.2) can be simplified as,

$$\hat{H} = -\frac{1}{2}\sum_{i}^{n}\nabla_i^2 - \frac{1}{2}\sum_{I}^{N}\sum_{i}^{n}\frac{Z_I}{|r_i - R_I|} + \frac{1}{2}\sum_{i}^{n}\sum_{j\neq i}^{n}\frac{1}{|r_j - r_i|} + \frac{1}{2}\sum_{I}^{N}\sum_{J\neq I}^{N}\frac{Z_I Z_J}{|R_J - R_I|} \quad (2.3)$$

Assuming the last term in Equation (2.3) to be constant, the electronic Hamiltonian is given as,

$$\hat{H} = \hat{T} + \hat{V}_{ext} + \hat{V}_H \quad (2.4)$$

where, $\hat{T}$ is the kinetic energy of the electrons, $\hat{V}_{ext}$ is the external potential due to nuclei and electron attraction and $\hat{V}_H$ is the Hartree potential due to electron-electron repulsion.

2.1.3 Hohenberg-Kohn Theorems

Even after implementing the Born-Oppenheimer approximation, it is time consuming and difficult to solve Equation (2.1). This is mainly because the electron wave-function depends on three spatial coordinates of each electron in a system that consists of n electrons. Hence, the dimensions of the wave-function scales up as $3n$. Instead of considering the solution in terms of wave-functions, electron density can be utilized in order to simplify the problem. This is the main reason for naming this approach as density functional theory.

The wave-function for a particular set of coordinates cannot be observed directly. Instead, the quantity that can be measured is the probability of finding the electrons in a particular set of coordinates. This probability is equal to the square of wave-function and is related to the electron density $\rho(\mathbf{r})$ as,

$$\rho(\mathbf{r}) = \sum_{i} |\psi_i^*(\mathbf{r})\psi_i(\mathbf{r})| \quad (2.5)$$

where, $\psi_i(\mathbf{r})$ is the single electron wave-function and the summation is over the occupied orbitals. $\rho(\mathbf{r})$ is a function of only three spatial coordinates, thereby reducing the dimensions of the problem tremendously. It should be noted that in DFT, $\rho(\mathbf{r})$ is used as the fundamental quantity rather than $\psi_i(\mathbf{r})$.

Hohenberg and Kohn (H-K) [Hohenberg and Kohn, 1964] stated two mathematical theorems, which laid the foundation for DFT. The first H-K theorem states that the ground state energy i.e., the lowest energy state of a system obtained by solving the Schrödinger equation, is a unique functional of $\rho(\mathbf{r})$.

$$E_0 = E[\rho(\mathbf{r})] \tag{2.6}$$

where, E_0 is the ground state energy. There is a one-to-one mapping that exists between the $\psi(\mathbf{r})$ and $\rho(\mathbf{r})$ at E_0. The second H-K theorem states that the electron density that corresponds to the full solution of the Schrödinger equation is the true electron density that relates to the global minimum of the energy functional.

$$E[\rho(\mathbf{r})] \geq E[\rho_0(\mathbf{r})] \tag{2.7}$$

where, $\rho_0(\mathbf{r})$ is the ground state electron density. This requires the knowledge of exact functional form of E so that E_0 can be found by varying $\rho(\mathbf{r})$.

2.1.4 Kohn-Sham Equation

The H-K theorems proposed a simplified way to solve the Schrödinger equation. On the other hand, the exact form of the energy functional and the procedure to obtain E_0 directly from $\rho(\mathbf{r})$ is still not known. The equations derived by Kohn and Sham [Kohn and Sham, 1965] were able to address this issue and hence, led to a major breakthrough in DFT. A fictitious system of electrons with an electron density same as that of the real system was introduced. The energy functional of such a system is given as,

$$\begin{aligned} E[\rho(\mathbf{r})] = &-\frac{1}{2}\int \psi_i^* \nabla^2 \psi_i \, \mathrm{d}^3 r + \int \hat{V}_{ext}(\mathbf{r})\rho(\mathbf{r}) \, \mathrm{d}^3 r \\ &+ \frac{1}{2}\int\int \frac{\rho(\mathbf{r})\rho(\mathbf{r}')}{|\mathbf{r}-\mathbf{r}'|} \, \mathrm{d}^3 r \, \mathrm{d}^3 r' + \Delta\hat{T}[\rho(\mathbf{r})] + \Delta\hat{V}_H[\rho(\mathbf{r})] \end{aligned} \tag{2.8}$$

The first term in Equation (2.8) represents the kinetic energy of the system. The second term denotes the external potential due to the attraction between the electrons and nuclei.

The third term is the coulombic repulsion between a pair of electrons. $\Delta\hat{T}[\rho(\mathbf{r})]$ and $\Delta\hat{V}_H[\rho(\mathbf{r})]$ represents the difference in kinetic and electron-electron interaction energy between the fictitious and real systems, respectively. The last two terms in Equation (2.8) along with other quantum mechanical effects that are not known, constitute the exchange correlation functional $E_{XC}[\rho(\mathbf{r})]$, which is given as,

$$E_{XC}[\rho(\mathbf{r})] = \Delta\hat{T}[\rho(\mathbf{r})] + \Delta\hat{V}_H[\rho(\mathbf{r})] \tag{2.9}$$

The most difficult challenge in DFT is modelling $E_{XC}[\rho(\mathbf{r})]$. There are several approximations for doing this. Some of the well known approximations are Local Density Approximation (LDA) [Kohn, 1986], Generalized Gradient Approximation (GGA) [Perdew and Levy, 1983], B3LYP (hybrid) [Becke, 1993], etc. A classification of these approximations has been illustrated using a Jacob's ladder, which is explained in the review by [Perdew and Schmidt, 2001]. There are different approximations available within GGA. The most widely used are GGA-PBE [Perdew et al., 1996] and GGA PW91 [Burke et al., 1998].

If $E_{XC}[\rho(\mathbf{r})]$ is defined using any approximation, the mathematical form of the Kohn-Sham (K-S) equation can be evaluated. From the K-S equation, one-electron operators were defined such that the single electron wave-functions for a fictitious system, also known as Kohn-Sham orbitals can be found by solving:

$$\left(-\frac{1}{2}\nabla_i^2 + \hat{V}_{ext}(\mathbf{r}) + \hat{V}_H(\mathbf{r}) + \hat{\mathbf{V}}_{XC}(\mathbf{r})\right)\psi_i(\mathbf{r}) = \varepsilon_i\psi_i(\mathbf{r}) \tag{2.10}$$

where, ε_i is the energy of the Kohn-Sham orbital and $\hat{V}_{XC}(\mathbf{r})$ is the exchange-correlation potential, which is a functional derivative of $E_{XC}[\rho(\mathbf{r})]$. $\hat{V}_H(\mathbf{r})$ includes the self-interaction of an electron with itself. The correction for self-interaction is included in the exchange correlation potential along with other corrections. Using Equation (2.10), the problem of finding the electron density is reduced to finding a set of single electron wave-functions, $\psi(\mathbf{r})$. The procedure of finding solutions to the K-S equation is known as the Self-Consistent Field (SCF) method, which will be explained in Section 2.3.

2.1.5 Plane waves and Blöch's theorem

Plane wave basis sets are used for representing the wave-functions in periodic solids. These wave-functions must satisfy the Blöch's theorem. It states that the wave-function for a periodic solid is a product of the plane wave and a periodic function with the same periodicity of the lattice.

$$\psi_{\mathbf{k}}(\mathbf{r}) = e^{i\mathbf{k}\cdot\mathbf{r}} \cdot u_{\mathbf{r}}(\mathbf{r}) \tag{2.11}$$

where, k is the wavevector, $\psi_{\mathbf{k}}(\mathbf{r})$ is the wavefunction, $e^{i\mathbf{k}\cdot\mathbf{r}}$ is the plane wave and $u_{\mathbf{r}}(\mathbf{r})$ is the periodic function. The periodic function can be expanded as,

$$u_{\mathbf{r}}(\mathbf{r}) = \sum_{\mathbf{G}_m} c_{\mathbf{G}_m} e^{i\mathbf{G_m}\cdot\mathbf{r}} \tag{2.12}$$

where, $\mathbf{G}_m$ are vectors of the reciprocal space and $c_{\mathbf{G}_m}$ is the plane wave expansion coefficient. Reciprocal vectors are defined as $\mathbf{G}_m = m_1 b_1 + m_2 b_2 + m_3 b_3$ where, m_1, m_2 and m_3 are real integers. Hence, the wavefunction for a periodic solid can be written as,

$$\psi_{\mathbf{k}}(\mathbf{r}) = \sum_{\mathbf{G}_m} c_{(\mathbf{G}_m+\mathbf{k})} e^{i(\mathbf{G_m}+\mathbf{k})\cdot\mathbf{r}} \tag{2.13}$$

Equation (2.13) shows that the wavefunctions differing by a reciprocal lattice vector $\mathbf{G}_m$, denotes the same wavefunction.

Energy cutoff

The K-S equations can be independently solved at each k-point with the wavefunction extending over infinite number of $\mathbf{G}_m$ vectors. But, it is not possible to use all the terms in the expansion due to the limitations in the computational resources. Hence, the plane wave basis set should be truncated at particular point. The solutions to K-S equations consists of kinetic energy terms of the form $\frac{1}{2}|\mathbf{k}+\mathbf{G}|^2$. Hence, the energy cutoff (E_{cut}) can be defined to truncate the wavefunction, when the following condition is satisfied (Equation (2.14)),

$$E_{cut} \geq \frac{1}{2}|\mathbf{k}+\mathbf{G}|^2 \tag{2.14}$$

k-point sampling

The integrals in K-S equations are evaluated in the reciprocal space *(k-space)*. The integration is performed only in the first Brilluion Zone (BZ) since the **k** vectors are unique in this BZ. The integral can be approximated such that it can be evaluated over a set of discrete points in the BZ. These sets of points define a k-point grid. One of the approaches for choosing an appropriate k-point grid for a particular structure is the Monkhorst-Pack method [Monkhorst and Pack, 1976].

2.1.6 Pseudopotentials

An atom consists of core and valence electrons. The core electrons are tightly bound to the nucleus while the valence electrons take part in the bonding. The wavefunctions oscillate rapidly near the core electrons and hence, higher (E_{cut}) values are required to represent a plane wave basis set. It can assumed that the core electrons are frozen along with the nucleus (frozen core approximation). This results in a non-oscillatory and smooth wavefunctions for the core electrons which are called the pseudo-wavefunctions with an effective potential known as pseudopotential [Phillips, 1958] [Phillips and Kleinman, 1959] Figure 2.1.

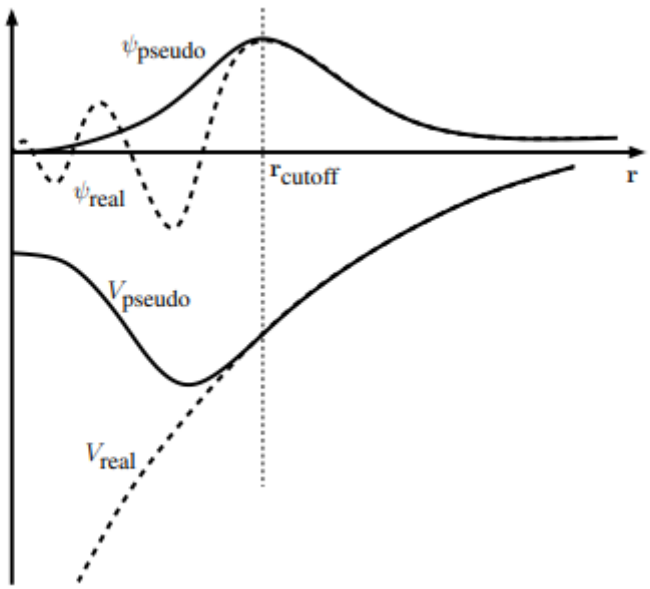

Figure 2.1: Pseudopotential approach

The pseudopotential of an atom should be transferable i.e., they should reproduce various chemical environments in which the atom is present. The pseudopotential and pseudo-wavefunctions must agree with the real wavefunction and potential, beyond a certain cutoff radius as shown in Figure 2.1. There are different types of pseudopotentials available in literature. The commonly used potentials are ultra-soft [Vanderbilt, 1990] and Projector Augmented Wave (PAW) pseudopotentials [Blöchl, 1994]; [Kresse and Joubert, 1999]. The PAW method combines the full-electron as well as pseudopotential approaches and requires higher (E_{cut}). Hence, they are known as hard pseudopotentials.

2.2 Total Energy Calculations

Total energy calculations of solids, based on DFT, requires only knowledge of crystal structure and yields quantities related to the electronic structure and total energy of a given structure at 0 K.

There are two tasks that can be specified as the primary objective of the calculation. The first of these is fixed cell calculation or a single point energy calculation, which gives the total ground state energy of the system along with the forces and stresses on the atoms. The second is variable cell calculation or a geometry optimization where the atoms are allowed to move, and from this the program calculates the geometry of the cell which minimizes the energy and stress to some set level of tolerance.

2.2.1 Fixed Cell Calculation

To get the accurate total energy, optimal E_{cut} and k-point grid are necessary. Fixed cell or single point energy calculation is used to calculate those.

The number of plane wave basis set included in the calculation is controlled by the cut-off energy (E_{cut}). Increasing the value of E_{cut} increases the accuracy at the expense of computation time. It is crucial to repeat the calculation a few times with increasing step size at a fixed k-point grid.

E_{cut} depends upon the type of atom and not the numbers. When performing convergence

calculation for E_{cut} for a system, k-point is kept constant. The curve E_{cut} vs. total energy is not always smooth. Force and stress convergence are more useful criterion. Energy minimum implies force is zero, but not vice versa. Forces usually converge at a lower cutoff than total energy because density in region of nucleus is unimportant. The high kinetic energy plane wave states are most important for the core states and these are relatively unchanged by their chemical environment. Therefore, selected cutoff energy should be same for all reactants and products. The errors due to finite cutoff energy tend to cancel out in the energy of formation.

The energy convergence w.r.t. k-point sampling needs to be studied for each material independently, i.e., for reactants and products. Since the Fermi surface of a compound can be completely different to those of its constituent elements; e.g. NaCl is an insulating material which require only a few k-points, whereas Na metal needs huge k-points and chlorine is an insulating molecular gas which requires only one k-point.

2.2.2 Variable Cell Calculation

During a geometry optimization, the lattice parameter may increase or decrease which depends on the starting point, and the degree of convergence of basis sets, k-points for Brillouin zone sampling, etc. There is also some pseudopotential error. So a fully converged cell optimization will give slightly different results depending on your starting point and choice of pseudopotentials. The geometry optimization convergence thresholds for energy change, maximum force, maximum stress, and maximum displacement between optimization cycles. The optimization will stop when all of these criteria are satisfied.

Chapter 3

Critical Review

3.1 Binary Systems

3.1.1 Ni-Ti System

The most recently assessed phase diagram of Ni-Ti binary system shows the presence of three intermediate phases which are BCC Ni_3Ti, FCC NiTi and HCP $NiTi_2$. The binary system was first studied by [Kaufman and Nesor, 1978]. It has been further evaluated by [Saunders and Chandrasekaran, 1992], [Haiyan and Zhanpeng, 1993], [Bellen et al., 1996], [Tokunaga et al., 2007], [Santhy and Kumar, 2010], [Tang et al., 1999]. In the evaluation by [Murray, 1987], three intermetallic compounds were formed: Ni_3Ti, NiTi and $NiTi_2$. Ni_3Ti and NiTi are melted congruently, while $NiTi_2$ was formed as a peritectic alloy. Ni_3Ti had no homogeneity.

[Jia et al., 1994] reported a homogeneity range for the Ni_3Ti phase.[Haiyan and Zhanpeng, 1993] modeled the NiTi phase using the Wagner-Schottky model to describe the homogeneity range, but treated Ni_3Ti phase as a line compound. The system has been thermodynamically evaluated by [Kaufman and Nesor, 1978], [Saunders and Chandrasekaran, 1992], [Bellen et al., 1996], [Tang et al., 1999] by using sublattice formula to account for the homogeneity of Ni_3Ti and NiTi phase.

Ni_3T was studied via sublattice model. The formula $(Ni,Ti)_{0:75}(Ni,Ti)_{0:25}$ was used for the Ni_3Ti phase. On the other hand, NiTi phase was studied with a CsCl-type B2 structure.

In the study by [Tokunaga et al., 2007] NiTi phase was treated as an independent phase. Similar model was used by [Santhy and Kumar, 2010] in modelling the Ni-Ti system for evaluation of a ternary compound.

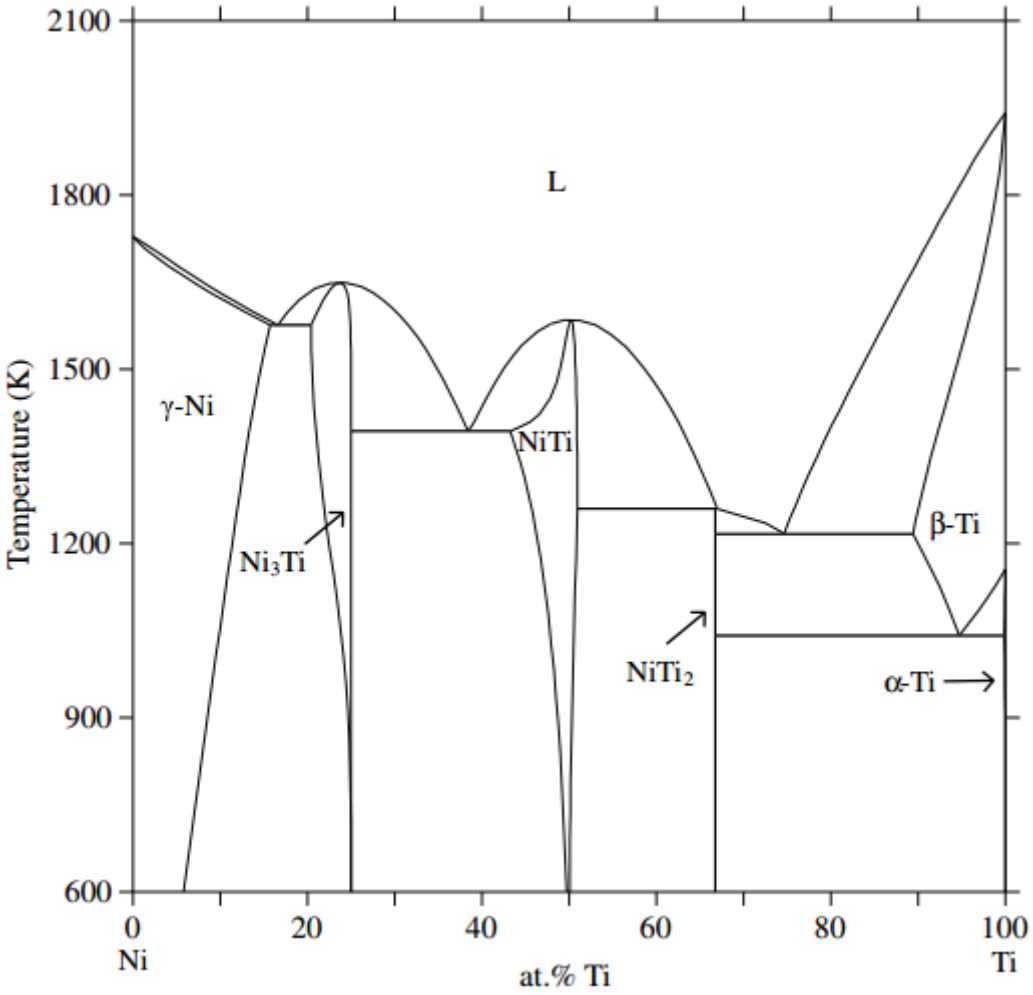

Figure 3.1: Nickel - Titanium Phase Diagram

Reaction	*Temperature(K)*
$L \rightleftharpoons NiTi$	1583
$Ni_3Ti \rightleftharpoons L+NiTi$	1393
$NiTi \rightleftharpoons L+NiTi_2$	1259

Table 3.1: Invariant reactions in Ni-Ti Binary System

3.1.2 Ni-Zr System

The system consists of eight thermodynamically stable intermediate phases: Ni_5Zr, Ni_7Zr_2, Ni_3Zr, $Ni_{21}Zr_8$, $Ni_{10}Zr_7$, $Ni_{11}Zr_9$, NiZr, and $NiZr_2$. Their crystal structures are well-established. Out which Ni_7Zr_2, NiZr and $NiZr_2$ melts congruently around 1713K, 1533K and 1393K respectively. Ni-Zr system was critical reviewed by [Nash, 1991] with experimental data upto year 1983. A thermodynamic description of the Ni-Zr system was reported by [Saunders and Chandrasekaran, 1992] but two intermediate phases, Ni_3Zr and $Ni_{11}Zr_9$, were not considered in the calculation.

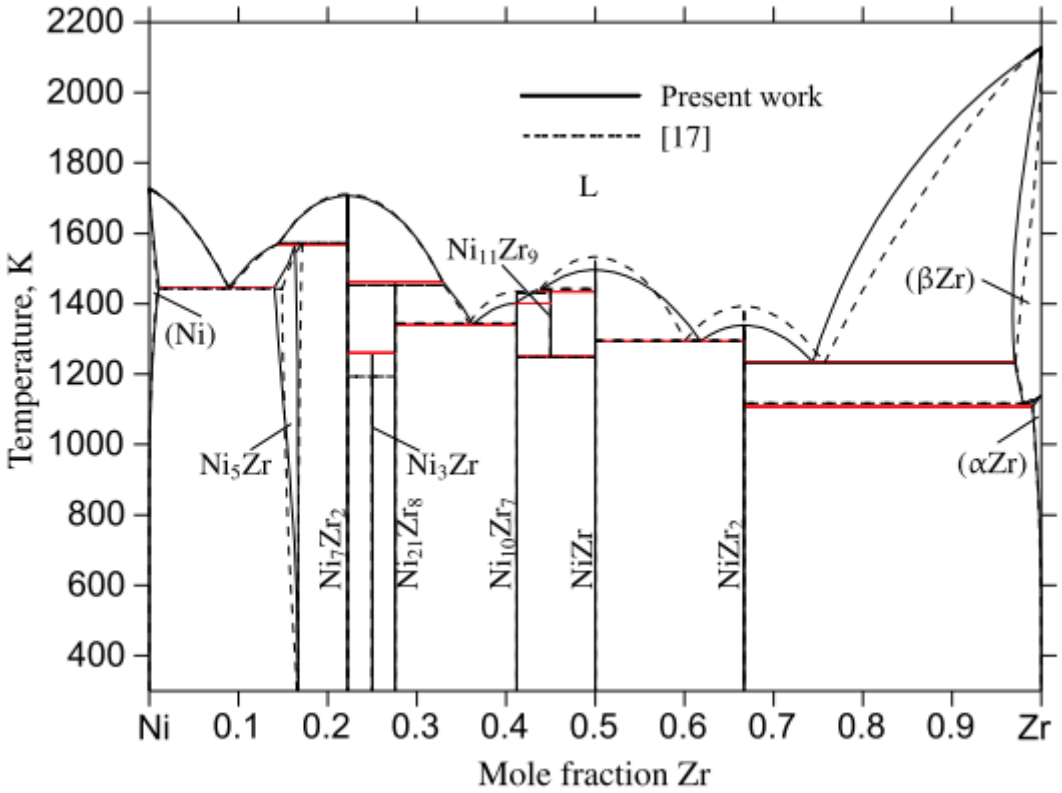

Figure 3.2: Nickel - Zirconium Phase Diagram

Reaction	*Temperature(K)*
$L + Ni_7Zr_2 \rightleftharpoons Ni_5Zr$	1569
$L + Ni_7Zr_2 \rightleftharpoons Ni_{21}Zr_8$	1462
———	—-

Reaction	*Temperature(K)*
———————————	—-
$L \rightleftharpoons Ni + Ni_5Zr$	1447
$L + NiZr \rightleftharpoons Ni_{11}Zr_9$	1434
$L + Ni_{11}Zr_9 \rightleftharpoons Ni_{10}Zr_7$	1401
$L \rightleftharpoons Ni_{21}Zr_8 + Ni_{10}Zr_7$	1340
$L \rightleftharpoons NiZr + NiZr_2$	1293
$Ni_7Zr_2 + Ni_{21}Zr_8 \rightleftharpoons Ni_3Zr$	1261
$Ni_{11}Zr_9 \rightleftharpoons Ni_{10}Zr_7 + NiZr$	1250
$L \rightleftharpoons NiZr_2 + (\beta\ Zr)$	1235
$(\beta\ Zr) \rightleftharpoons NiZr_2 + (\alpha\ Zr)$	1108
$L \rightleftharpoons Ni_7Zr_2$	1707
$L \rightleftharpoons NiZr$	1496
$L \rightleftharpoons NiZr_2$	1339

Table 3.2: Invariant reactions in Ni-Zr Binary System

3.1.3 Ti-Zr System

Ti-Zr system is homogeneous system throughout the range with three phases namely liquid, (βTi, βZr) and (αTi, αZr) with two invariant reactions.

The system has been thermodynamically evaluated by []Hari Kumar14 which improvised the previous accepted version and was now in better agreement with experimental results. The system was recently assessed by [Sridar et al., 2017] which revised the gibbs energy description to have a better agreement with experimental enthalpy of mixing reported by [Thiedemann et al., 1999] which concluded that the invariant reaction ($L \rightleftharpoons (\alpha Zr)+(\beta Zr)$) fits better as an eutectic reaction.

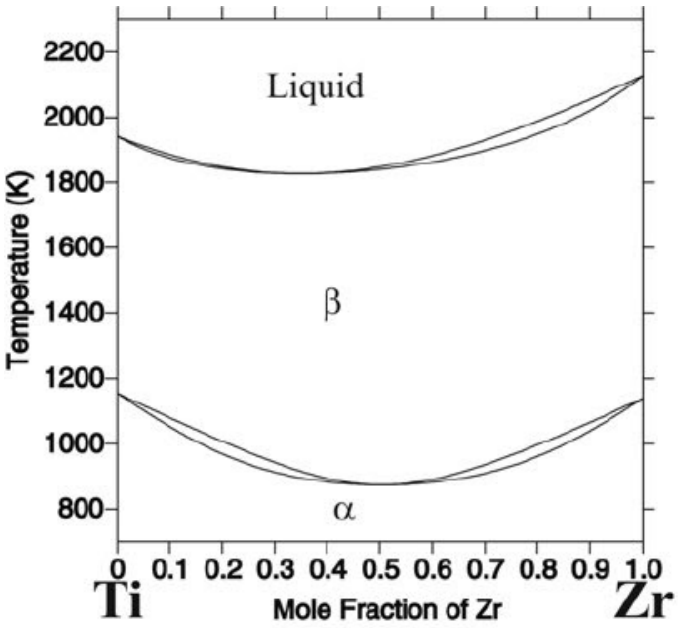

Figure 3.3: Titanium - Zirconium Phase Diagram

3.2 Ni-Ti-Zr Ternary system

[Van Vucht, 1966] reported the presence of a 9-layered BaPba structure (hhc) with some homogeneity region in the compositions ranging from Ni3(Ti0.75.Zr0.25) to Ni3(Ti0.5,Zr0.5). The lattice constants were a = 6.961 A, = 43'30' (the hexagonal unit cell a = 5.158 A, c = 18.875 A, c/a = 3.66). Annealing, however, at temperatures below 1300 °C resulted in a decomposition of this phase into a Ni3Ti-type structure and an unknown structure which has an X-ray diagram isotypic with the one obtained for the composition Ni_3Zr. The ternary system of Ni-Ti-Zr was previously critically reviewed by [Gupta, 1999]. In the Ni-Ti-Zr two ternary compound phase, a $MgZn_2$-type Laves phase, NiTiZr and Ni_3(Ti0:67Zr0:33) with a $BaPb_3$-type structure, were reported in the review by [Gupta, 1999]. The temperature and composition range stability for the NiTiZr compound has been studied by [Tokunaga et al., 2007]. There is a discrepancy related to the solubility range. Omitted the other ternary phase due to discrepancy in the thermodynamic data. Experimental study was required to determine the solid solubility of Zr in NiTi. NiTiZr phase show an extension in the $NiTi_2$ phase experimentally (but Laves Phase modelling does not support this).

Further experimental studies done by [Yeh et al., 2014] and [Liu et al., 2015] provide the

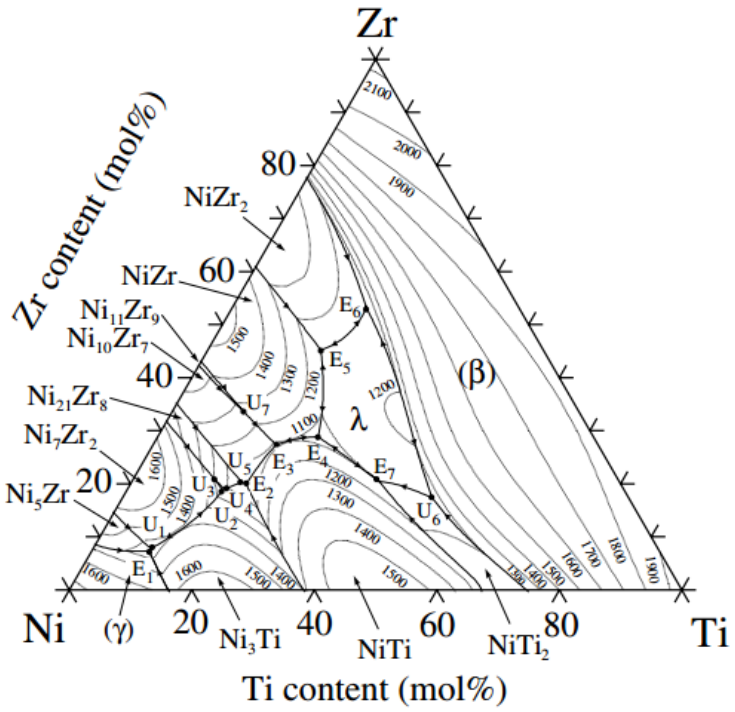

Figure 3.4: Nickel - Titanium - Zirconium Phase Diagram

temperature range stability and as well as the thermodynamic equilibrium of NiTiZr with other phases upto 1200 °C. The study also confirms the presence of the NiTiZr phase at low Temperature range along with the presence of the liquid phase.The studies also support the extension of NiTiZr in $NiTi_2$ with certain solubility around 800 °C. The composition range of the ternary phase is $Ni_xTi_yZr_z$, in which x ∈ [27,42], y ∈ [26-57], z ∈ [20-40], x + y + z = 100 around 800 °C [Yeh et al., 2014]. The other ternary phase Ni3(Ti0:67Zr0:33) was reported by [Van Vucht, 1966] around 1500 °C. It wasn't reported in the experimental studies performed by (Ref - 2013 , 2015) which suggest that it is present only at temperature (> 1300).

[Liu et al., 2015] has reported four equilibrium around 1200 °C Which are as follows:

- Ni_3Ti + NiZr + L
- Ni_3Ti + Ni + Ni_5Zr
- Ni_3Ti + Ni_7Zr_2 + Ni_5Zr
- L + Ni_5Zr + Ni

Type	*Reaction*	*Temperature(K)*	*Composition of Liquid Phase (mol%)*	
			Ti	Zr
E_1	$L \rightleftharpoons \gamma + Ni_3Ti + Ni_5Zr$	1335	9.4	7.7
E_2	$L \rightleftharpoons NiTi + Ni_3Ti + Ni_{10}Zr_7$	973	18.9	20.1
E_3	$L \rightleftharpoons NiTi + NiZr + Ni_{10}Zr_7$	1085	20.1	27.4
E_4	$L \rightleftharpoons NiTi + NiZr + \lambda$	1055	26.1	29.0
E_5	$L \rightleftharpoons NiZr + NiZr_2 + \lambda$	1100	18.5	45.1
E_6	$L \rightleftharpoons \beta + NiZr_2 + \lambda$	1098	21.8	53.0
E_7	$L \rightleftharpoons NiTi + NiTi_2 + \lambda$	1098	40.2	20.6
U_1	$L + Ni_7Zr_2 \rightleftharpoons Ni_3Ti + Ni_5Zr$	1339	9.6	8.1
U_2	$L + Ni_7Zr_2 \rightleftharpoons Ni_3Ti + Ni_3Zr$	1132	15.7	19.0
U_3	$L + Ni_7Zr_2 + Ni_{21}Zr_8 \rightleftharpoons Ni_3Zr$	1136	13.6	20.8
U_4	$L + Ni_3Zr \rightleftharpoons Ni_3Ti + Ni_{21}Zr_8$	1118	15.8	19.2
U_5	$L + Ni_{21}Zr_8 \rightleftharpoons Ni_3Ti + Ni_{10}Zr_7$	986	18.0	20.4
U_6	$L + \beta \rightleftharpoons NiTi_2 + \lambda$	1134	50.3	17.5
U_7	$L + Ni_{11}Zr_9 \rightleftharpoons NiZr + Ni_{10}Zr_7$	1267	11.4	33.9

Table 3.3: Invariant reactions in Ni-Ti-Zr Ternary System

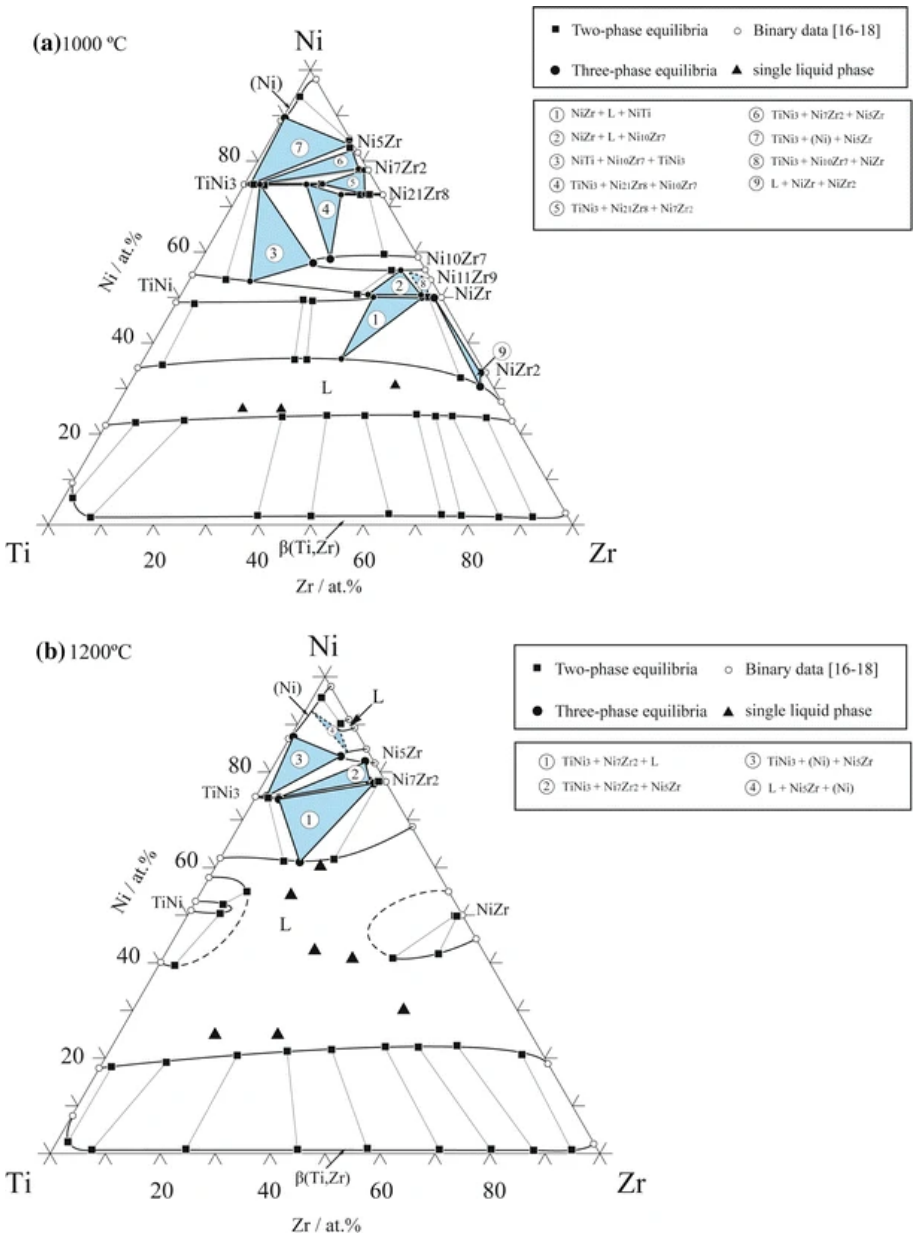

Figure 3.5: Nickel - Titanium -Zirconium Isothermal Section at 1000 °C and 1200 °C

Chapter 4

Softwares and Platform Involved

4.1 Crytallographic Information File (CIF)

The first step in our study is obtaining the crystallographic data. Crystallographic Information File (CIF) can be obtained from any of the open source crystallographic databases like bilbao, materials project etc.

Listing 4.1: *Example CIF File*

```
NiTi CIF file
# generated using pymatgen
data_TiNi
_symmetry_space_group_name_H-M Cmcm
_cell_length_a 2.91782251
_cell_length_b 9.39590862
_cell_length_c 4.01415842
_cell_angle_alpha 90.00000000
_cell_angle_beta 90.00000000
_cell_angle_gamma 90.00000000
_symmetry_Int_Tables_number 63
_chemical_formula_structural TiNi
_chemical_formula_sum 'Ti4 Ni4'
_cell_volume 110.05053608
```

```
_cell_formula_units_Z 4
loop_
_symmetry_equiv_pos_site_id
_symmetry_equiv_pos_as_xyz
1 'x, y, z'
2 '-x, -y, -z'
3 '-x, -y, z+1/2'
4 'x, y, -z+1/2'
5 'x, -y, -z'
6 '-x, y, z'
7 '-x, y, -z+1/2'
8 'x, -y, z+1/2'
9 'x+1/2, y+1/2, z'
10 '-x+1/2, -y+1/2, -z'
11 '-x+1/2, -y+1/2, z+1/2'
12 'x+1/2, y+1/2, -z+1/2'
13 'x+1/2, -y+1/2, -z'
14 '-x+1/2, y+1/2, z'
15 '-x+1/2, y+1/2, -z+1/2'
16 'x+1/2, -y+1/2, z+1/2'
loop_
_atom_site_type_symbol
_atom_site_label
_atom_site_symmetry_multiplicity
_atom_site_fract_x
_atom_site_fract_y
_atom_site_fract_z
_atom_site_occupancy
Ti Ti0 4 0.000000 0.357253 0.750000 1
Ni Ni1 4 0.000000 0.085051 0.750000 1
```

4.2 VESTA (Visualisation for Electronic Structural Analysis)

The second step is extracting the required parameter data. VESTA is a 3D visualization program for structural models, volumetric data such as electron/nuclear densities, and crystal morphologies. Using this we can extract the required lattice parameter to perform the calculations.

Listing 4.2: *Example extracted data file from VESTA*

```
Extracted data file
ti4 ni4
1.0
2.9178225994 0.0000000000 0.0000000000
0.0000000000 9.3959083557 0.0000000000
0.0000000000 0.0000000000 4.0141582489
Ti Ni
4 4
Direct
0.000000000 0.357252994 0.750000000
0.000000000 0.642747031 0.250000000
0.500000000 0.857252969 0.750000000
0.500000000 0.142747018 0.250000000
0.000000000 0.085050999 0.750000000
0.000000000 0.914949001 0.250000000
0.500000000 0.585050999 0.750000000
0.500000000 0.414949001 0.250000000
```

4.3 XCrySDen

XCrySDen stands for Crystalline Structures and Densities and X because it runs under the X-Window environment. It is a molecular and crystalline - structure visualization program,

but its main function is as a property analyzer program. It can run on most UNIX platforms, without any special hardware or software requirements. Special efforts were made to allow for appropriate display of 3D iso-surfaces and 2D contours. XCrySDen is also a graphical user interface for the CRYSTAL (another *ab initio* software).It can perform real-time operations such as rotation and translation. A specialized periodic-structure visualization program must also possess additional specific features such as displaying the crystal cages (lattices) in direct and reciprocal space, and displaying the Wigner Seitz cell (direct space) and the first Brillouin zone (reciprocal space). Beside measuring the distances and angles, measurement of crystal planes is also supported.

4.4 Quantum Espresso

The density functional theory calculations in our thesis are performed using the software package Quantum ESPRESSO, which stands for opEn Source Package for Research in Electronic Structure, Simulation, and Optimization. It is freely available to researchers around the world under the terms of the GNU General Public License. The package includes functions such as self-consistent calculations and atomic relaxation (pw.x), postprocessing (pp.x), atomic-projection (projwfc.x), phonon calculation (ph.x) and Wannier generation (wannier90.x). For our work pw.x package was used to perform the self consistent calculations and atomic relaxation.

4.4.1 First Principle calculations

Based on Density Functional theory (DFT), from first principles one may calculate the energy at 0K for different configurations of atoms on specific lattices. These energies can be expanded in different ways to describe disordered states for compositions in between the calculated configurations. Computational softwares like Quantum ESPRESSO, CRYSTAL are used for these calculations.

Listing 4.3: *Quantam espresso input file description*

```
## Quantam espresso input file description ##
```

```
&CONTROL
Calculation : A string describing the task to be performed.
restart mode : From scratch. This is the normal way to perform a PWscf
    calculation
outdir : directory where the output result files should be stored
Pseudo dir : directory containing the pseudopotential needed for the
    calculations
Etoto_convo_thr : minimum convergence value.
nstep : no. of iterations

&SYSTEM
Ibrav : Bravais-lattice index. Specify which lattic used
nat : no. of atoms
ntype : no. of different types of atoms
a, b, c, : lattice parameters
ecutwfc : cutoff value for the plane wave
ecutrho : 8 - 12 times of ecutwfc
nspin : polarization ( if required)

&ELECTRONS
Conv_thr = Convergence threshold for selfconsistency
mixing_beta = mixing factor for self-consistency

ATOMIC SPECIES
Element on which calcultion is perfomed, its Mass and the corresponding
    pseudopotential file

ATOMIC POSITION crystal
atomic positions are in crystal coordinates, i.e. in relative coordinates
    of the primitive lattice
```

```
vectors as defined either in card CELL_PARAMETERS or via the ibrav + celldm
    / a,b,c... variables


K_POINTS automatic
automatically generated uniform grid of k-points, i.e, generates ( nk1, nk2,
    nk3 ) grid with ( sk1, sk2, sk3 ) offset. nk1, nk2, nk3 as in Monkhorst
   -Pack grids k1, k2, k3 must be 0 ( no offset ) or 1 ( grid displaced by
   half a grid step in the corresponding direction )
```

Steps Involved in First Principle Calculations

1. Modelling the input crystal structure based on the critical assessment. Quantum ESPRESSO(QE) an open source DFT code is used to perform the calculations and another open source visualizing software XcrySDen is used to visualize the input and output structure.

2. Performing DFT calculations for the modelled structure.

3. Optimising the obtained parameter by fine tuning the input.

Quantum Espresso also has a GUI called BURAI. It has all the necessary functionalities of Quantum ESPRESSO that we needed for our project work along with the added perk of being able to visualize the structure.

Chapter 5

Experimental Calculations

5.1 Elemental Calculations

5.1.1 Nickel

Input Figure

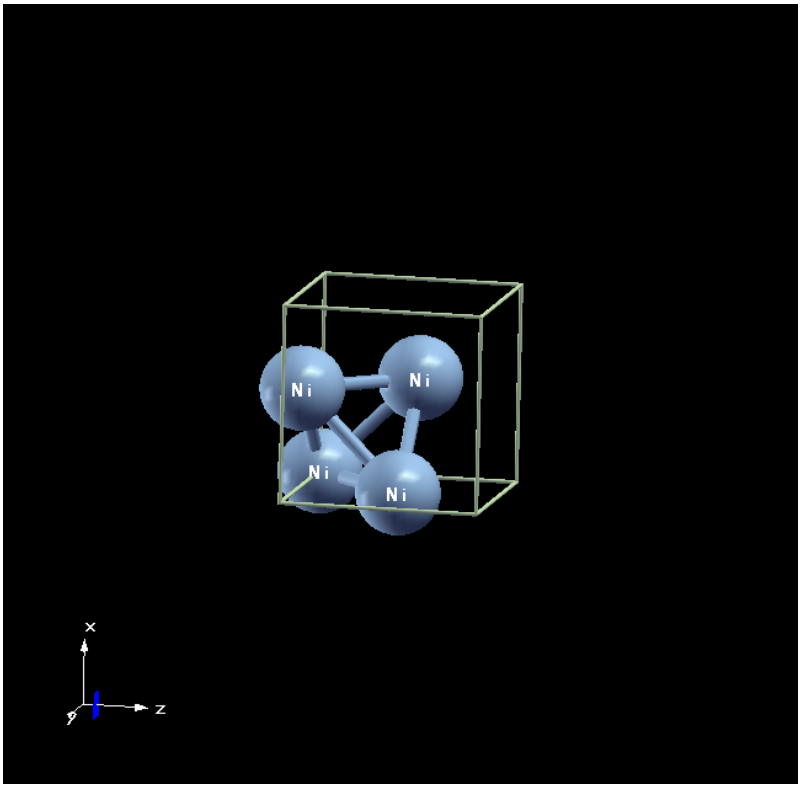

Figure 5.1: Input Structure for Nickel

Input File

Listing 5.1: *Elemental Calculation for Nickel*

```
&CONTROL
title = 'Ni_mp-23_conventional_standard.cif'
calculation = 'vc-relax'
restart_mode = 'from_scratch'
outdir = 'outdir2'
pseudo_dir = '/home/akhilesh/Desktop/Major_Project/DFT/Pseudopotential'
prefix = 'Ni_mp-23_conventional_standard'
disk_io = 'high'
etot_conv_thr = 0.0001
forc_conv_thr = 0.001
nstep = 400
 /
&SYSTEM
ibrav = 2
nat = 1
ntyp = 1
a = 3.524
b = 3.524
c = 3.524
ecutwfc = 75
ecutrho = 600
nspin = 2, starting_magnetization(1)=0.7,
occupations='smearing', smearing='marzari-vanderbilt', degauss=0.02
/
&ELECTRONS
conv_thr = 1.0e-8
mixing_beta = 0.7
/
```

```
&IONS
ion_dynamics = 'bfgs'
/
&CELL
cell_dynamics= 'bfgs',
/
ATOMIC_SPECIES
Ni   58.6934000000 Ni.pz-nd-rrkjus.UPF
ATOMIC_POSITIONS crystal
Ni      0.00000000000000    0.00000000000000    0.00000000000000
K_POINTS automatic
8 8 8  0 0 0
```

5.1.2 Zirconium

Input Figure

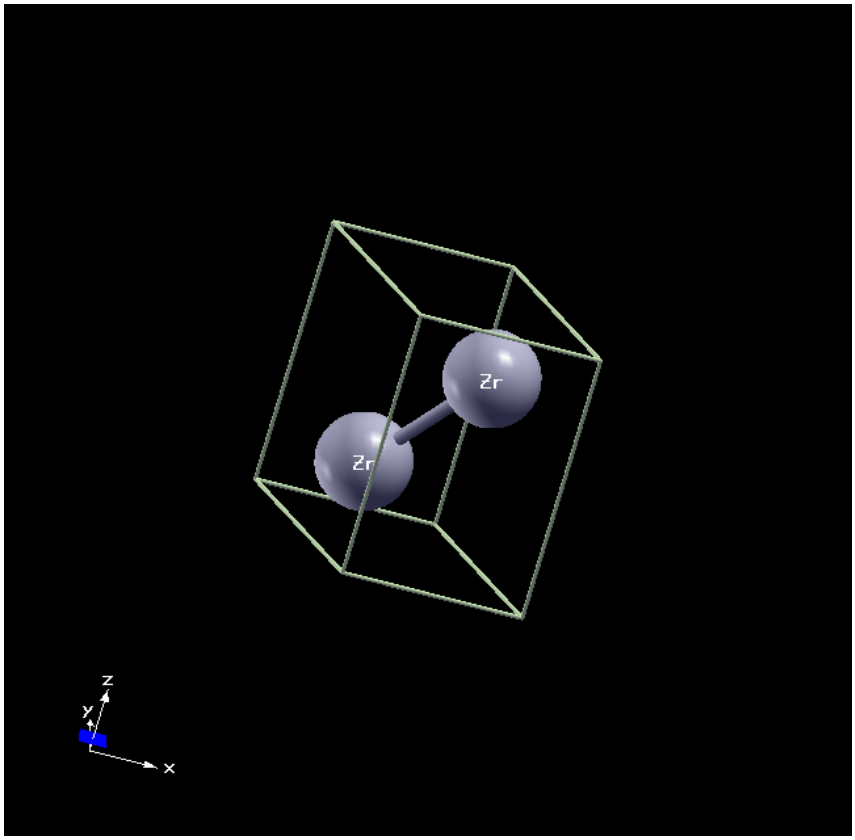

Figure 5.2: Input Structure for Zirconium

Input File

Listing 5.2: *Elemental Calculation for Zirconium*

```
&CONTROL
title = 'Zr.cif'
calculation = 'vc-relax'
restart_mode = 'from_scratch'
outdir = 'outdir'
pseudo_dir = '/home/akhilesh/Desktop/Major_Project/DFT/Pseudopotential'
prefix = 'Zr'
verbosity = 'default'
etot_conv_thr = 0.0001
forc_conv_thr = 0.001
/
&SYSTEM
ibrav = 4
nat = 2
ntyp = 1
a = 3.2392
b = 3.2392
c = 5.1722
ecutwfc = 95
ecutrho = 950
occupations = 'smearing',
smearing = 'methfessel-paxton',
degauss = 0.02
/
&ELECTRONS
diagonalization='david',
mixing_beta = 0.7
conv_thr = 1.0D-7,
```

```
electron_maxstep = 100
/
&IONS /
&CELL /
ATOMIC_SPECIES
Zr   91.2240000000 Zr.pbesol-spn-kjpaw_psl.1.0.0.UPF
ATOMIC_POSITIONS crystal
Zr      0.33333300000000    0.66666700000000    0.25000000000000
Zr      0.66666700000000    0.33333300000000    0.75000000000000
K_POINTS automatic
11  11  11   0 0 0
```

5.1.3 Titanium

Input Figure

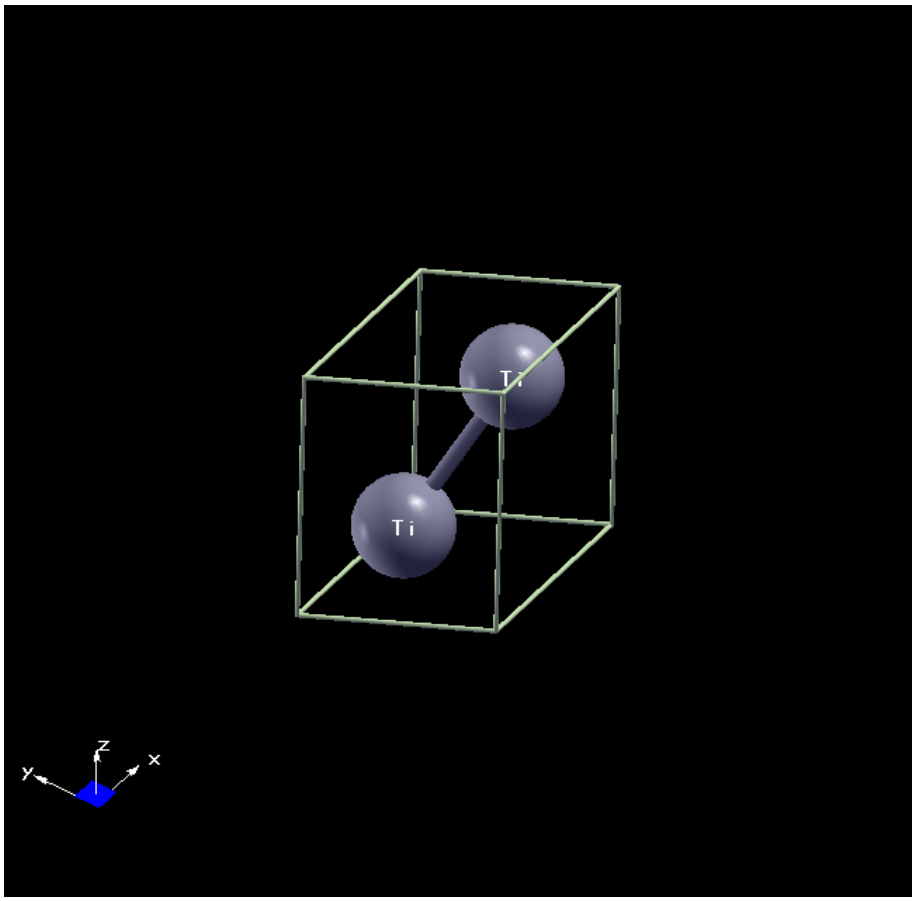

Figure 5.3: Input Structure for Titanium

Input File

Listing 5.3: *Elemental Calculation for Titanium*

```
&CONTROL
title = 'Ti_mp-72_conventional_standard.cif'
calculation = 'vc-relax'
restart_mode = 'from_scratch'
outdir = 'outdir1'
pseudo_dir = '/home/akhilesh/Desktop/Major_Project/DFT/Pseudopotential'
prefix = 'Ti_mp-72_conventional_standard'
verbosity = 'default'
etot_conv_thr = 0.0001
forc_conv_thr = 0.001
/
&SYSTEM
ibrav = 4
nat = 2
ntyp = 1
a = 2.943
b = 2.943
c = 4.698
ecutwfc = 90
ecutrho = 900
occupations = 'smearing',
smearing = 'methfessel-paxton',
degauss = 0.02
/
&ELECTRONS
diagonalization='david',
mixing_beta = 0.7
conv_thr = 1.0D-7,
```

```
electron_maxstep = 100
/
&IONS /
&CELL /
ATOMIC_SPECIES
Ti   47.8670000000 Ti.pbesol-spn-kjpaw_psl.1.0.0.UPF
ATOMIC_POSITIONS crystal
Ti      0.33333300000000    0.66666700000000    0.25000000000000
Ti      0.66666700000000    0.33333300000000    0.75000000000000
K_POINTS automatic
9  9  9   0 0 0
```

5.2 Binary System Calculations

5.2.1 Nickel-Titanium

Input Figure

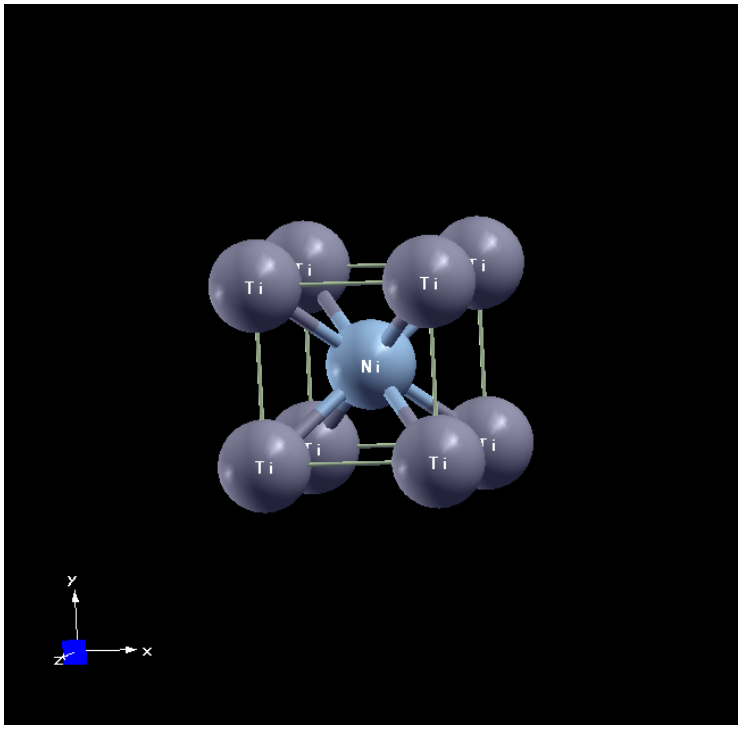

Figure 5.4: Input Structure for Nickel-Titanium

Input File

Listing 5.4: *Binary Calculation for Nickel-Titanium*

```
&CONTROL
title = 'TiNi_mp-1067248_conventional_standard.cif'
calculation = 'vc-relax'
restart_mode = 'from_scratch'
outdir = 'outdir1'
pseudo_dir = '/home/akhilesh/Desktop/Major_Project/DFT/Pseudopotential'
prefix = 'TiNi_mp-1067248_conventional_standard'
verbosity = 'default'
etot_conv_thr = 0.0001
forc_conv_thr = 0.001
/
&SYSTEM
ibrav = 3
nat = 2
ntyp = 2
ecutwfc = 90
ecutrho = 900
a = 3.015
b = 3.015
c = 3.015
occupations = 'smearing',
smearing = 'methfessel-paxton', degauss = 0.02
/
&ELECTRONS
diagonalization ='david',
mixing_beta = 0.7
conv_thr = 1.0D-7,
electron_maxstep = 100
```

```
/
&IONS /
&CELL/
ATOMIC_SPECIES
Ti   47.8670000000 Ti.pbesol-spn-kjpaw_psl.1.0.0.UPF
Ni   58.6934000000 Ni.pbesol-spn-kjpaw_psl.1.0.0.UPF
ATOMIC_POSITIONS crystal
Ni      0.500000     0.5000000      0.5000000
Ti      1.000000     0.0000000      0.0000000
K_POINTS automatic
9 9 9 0 0 0
```

5.2.2 Nickel-Zirconium

Input Figure

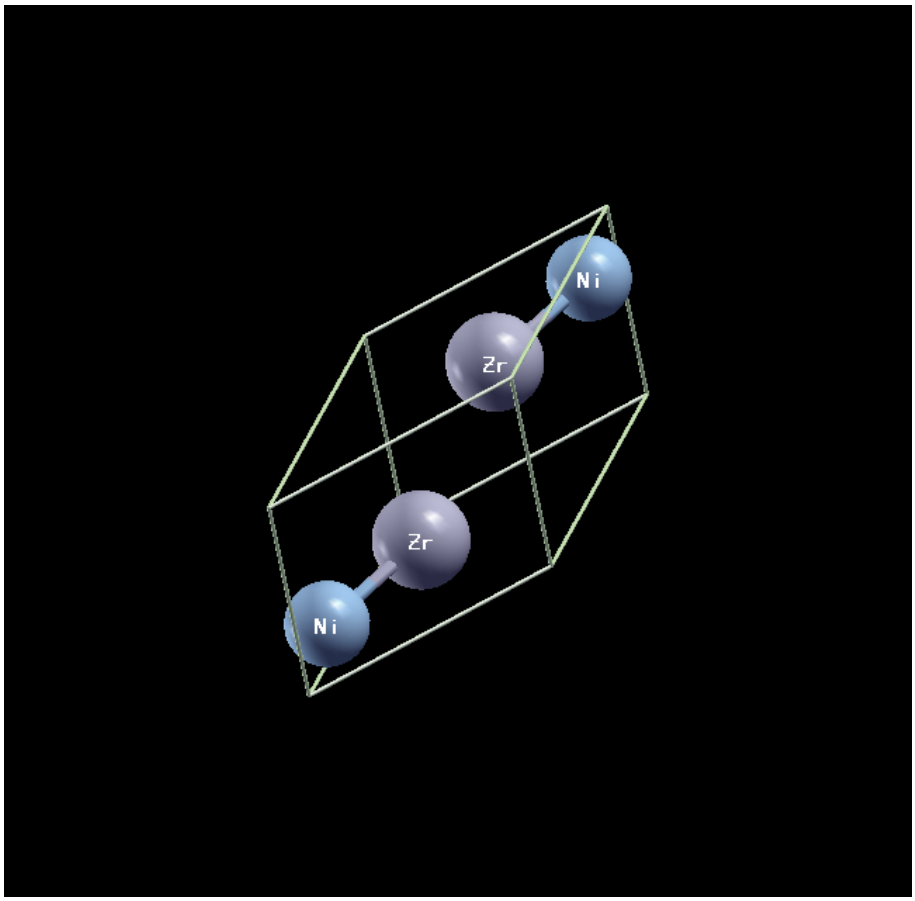

Figure 5.5: Input Structure for Nickel-Zirconium

Input File

Listing 5.5: *Binary Calculation for Nickel-Zirconium*

```
&CONTROL
title = 'ZrNi.cif'
calculation = 'scf'
restart_mode = 'from_scratch'
outdir = 'outdir1'
pseudo_dir = '/home/akhilesh/Desktop/Major_Project/DFT/Pseudopotential'
prefix = 'ZrNi'
etot_conv_thr = 0.0001
forc_conv_thr = 0.001
/
&SYSTEM
ibrav = 1
nat = 4
ntyp = 2
a = 5.2511
b = 5.2511a
c = 4.0855
ecutwfc = 85
ecutrho = 850
occupations = 'smearing',
smearing = 'methfessel-paxton', degauss = 0.02


/
&ELECTRONS
diagonalization='david',
mixing_beta = 0.7
conv_thr = 1.0D-7,
electron_maxstep = 100 /
```

```
&IONS/
&CELL /
ATOMIC_SPECIES
Ni   58.6934000000 Ni.pbesol-spn-kjpaw_psl.1.0.0.UPF
Zr   91.2240000000 Zr.pbesol-spn-kjpaw_psl.1.0.0.UPF

ATOMIC_POSITIONS crystal
Zr      0.360566 0.639434 0.750000
Zr      0.639434 0.360566 0.250000
Ni      0.082746 0.917254 0.750000
Ni      0.917254 0.082746 0.250000

K_POINTS automatic
5  5  5   0 0 0
```

Chapter 6

Results

6.1 Total Energy Calculation Results

1. Ni (FCC) = -426.5321 Ry (1 atom)
2. Ti (HCP) = -363.53821 Ry (2 atoms) (for 1 atom 363.53821/2 = 181.7691 Ry)
3. Zr (HCP) = -303.0994 Ry(1 atom)
4. NiTi (B2) = -608.4033 Ry (primitive cell - 1 Ni atom , 1 Ti atom)
5. NiZr (Orthorhombic) = -729.75205 Ry (primitive cell[triclinic]-1 Ni atom, 1 Zr atom)

6.2 Energy of Formation of Compounds

$$\Delta E_{A_pB_q} = \frac{1}{p+q}E_{A_pB_q} - \frac{p}{p+q}E_A - \frac{q}{p+q}E_B \tag{6.1}$$

$$\begin{aligned}
\Delta E_{NiTi} &= (NiTi(B2) - Ni(FCC - 1atom) - Ti(HCP - 1atom))/2 \\
&= (-608.4033 + 426.5821 + 181.7691)/2 \\
&= -0.02605Ry \\
&= -0.02605 * 1312.7496kJ/mol \\
&= -34.1971kJ/mol
\end{aligned}$$

$$\Delta E_{NiZr} = (NiZr(Primitive(triclicnic) - Ni(FCC - 1atom) - Zr(HCP - 1atom)/2$$
$$= (-729.75205 + 426.5821 + 303.0994)/2$$
$$= -0.035275Ry$$
$$= -0.035275 * 1312.7496kJ/mol$$
$$= -46.3072kJ/mol$$

6.3 Comparison with Literature Data

6.3.1 NiTi

Energy (kJ/mol)	*Reference*
34.20	This study
34.00 ± 2.0	[Gachon et al., 1981]
33.90 ± 2.0	[Kubaschewski, 1956]
32.51	[Yi and Moore, 1989]
33.10	[Guo and Kleppa, 1998]
36.00	[Pasturel et al., 1995]
36.10	[Santhy and Kumar, 2010]

Table 6.1: Comparison of Energy of Formation of NiTi with Literature data

6.3.2 NiZr

Energy (kJ/mol)	*Reference*
46.31	This study
48.53 ± 2.5	[Henaff et al., 1984]
46.70 ± 2.5	[Zaitsev et al., 2002]
48.24	[Watson and Bennett, 1981]
50.00	[Colinet et al., 1985]
50.87	[Zhang et al., 2007]
43.99	[Kirklin et al., 2015]
48.38	[Hennig et al., 2005]
46.23	[Jana et al., 2020]

Table 6.2: Comparison of Energy of Formation of NiZr with Literature data

6.4 Total Energy Calculation for single elements

6.4.1 Nickel

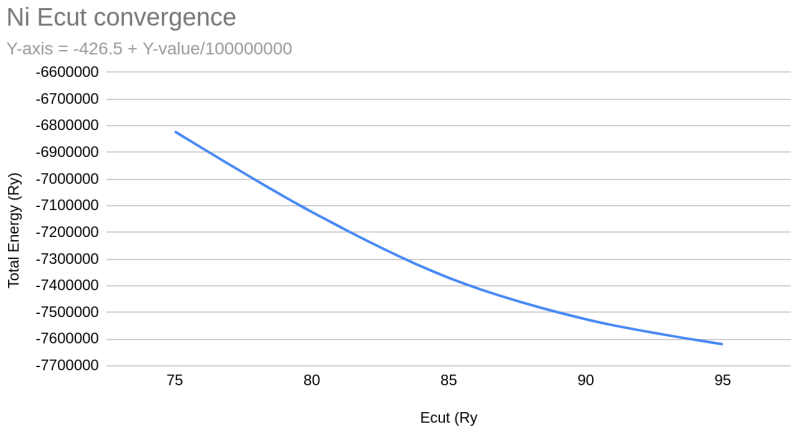

(a) E_{cut} Convergence

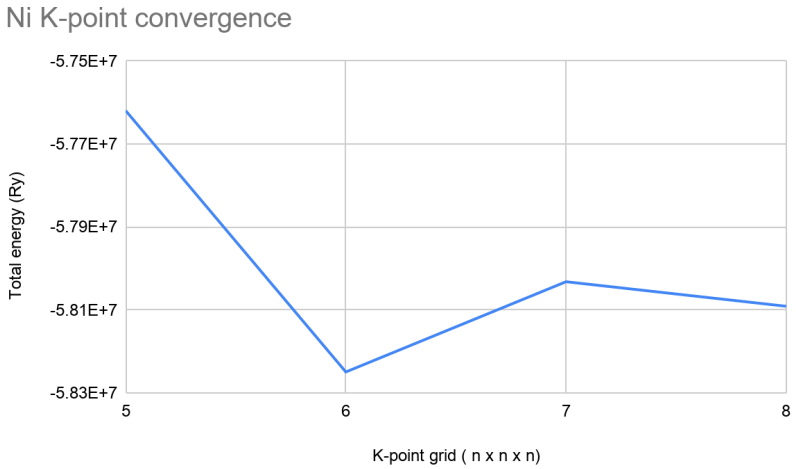

(b) k-point Convergence

Figure 6.1: Calculations for Nickel

Total Energy	$E_{cut}(Ry)$
-426.6821145	75
-426.7123023	80
-426.7370179	85
-426.7525620	90
-426.7619156	95

(a) E_{cut} Convergence

Total Energy	*k-points*
-576.19156	5
-582.49447	6
-580.31883	7
-580.91047	8

(b) k-point Convergence

Table 6.3: Convergence values for Nickel

6.4.2 Zirconium

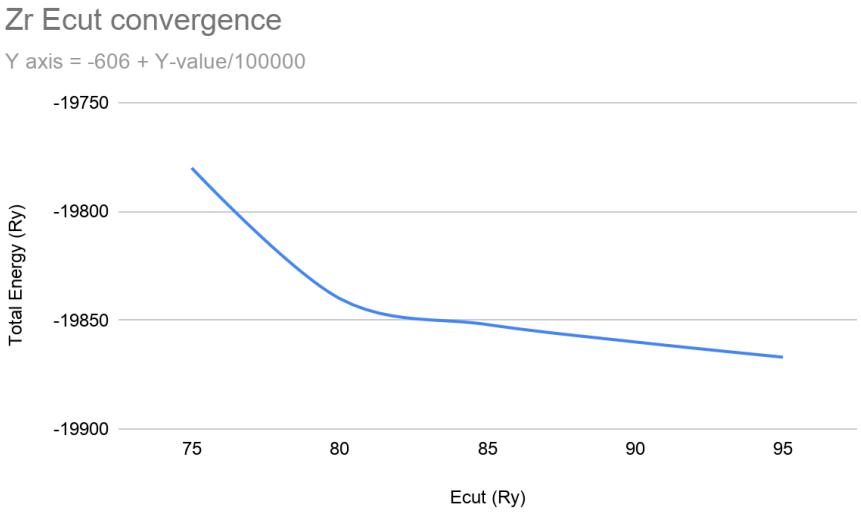

(a) E_{cut} Convergence

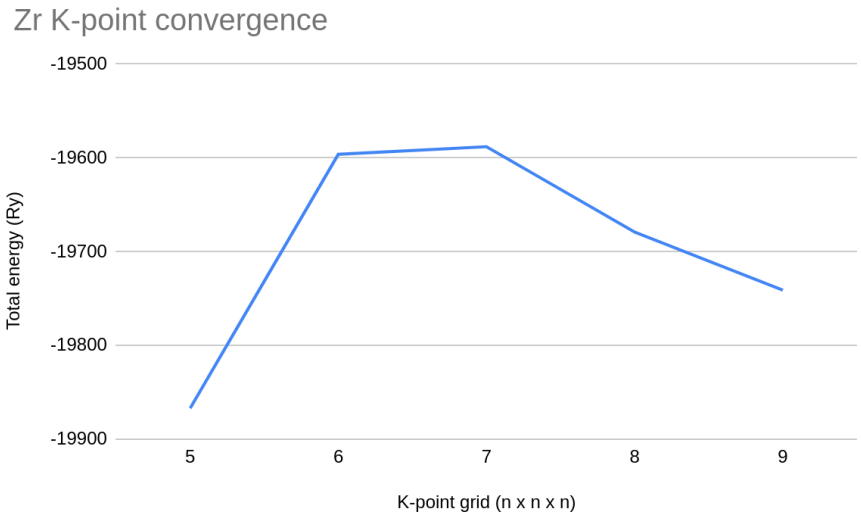

(b) k-point Convergence

Figure 6.2: Calculations for Zirconium

Total Energy	$E_{cut}(Ry)$
-606.19780	75
-606.19840	80
-606.19852	85
-606.19860	90
-606.19867	95

(a) E_{cut} Convergence

Total Energy	*k-points*
-606.19867	5
-606.19596	6
-606.19588	7
-606.19679	8
-606.19741	9

(b) k-point Convergence

Table 6.4: Convergence values for Zirconium

6.4.3 Titanium

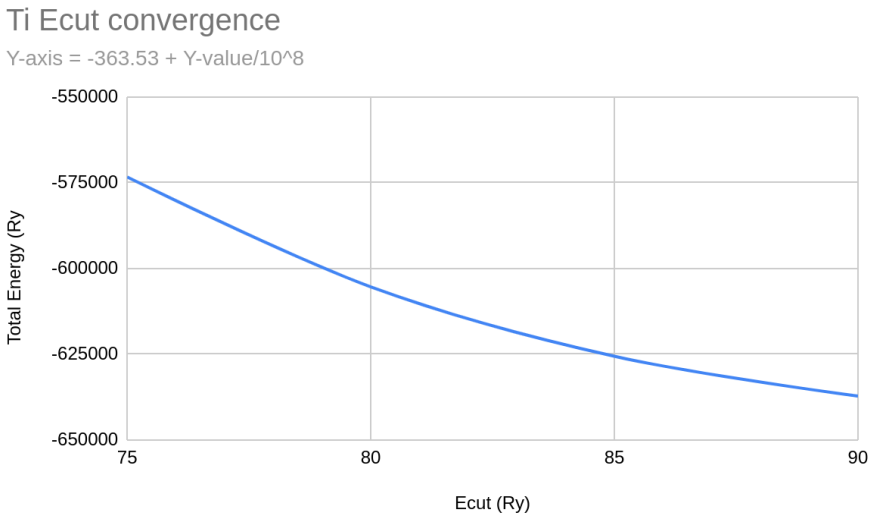

(a) E_{cut} Convergence

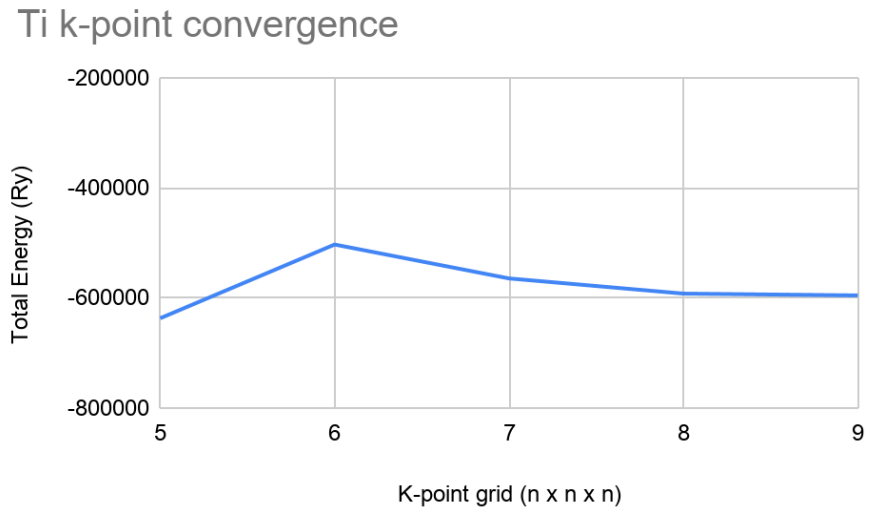

(b) k-point Convergence

Figure 6.3: Calculations for Titanium

Total Energy	$E_{cut}(Ry)$
-363.573333	75
-363.605352	80
-363.625587	85
-363.637188	90

(a) E_{cut} Convergence

Total Energy	*k-points*
-363.637188	5
-363.502967	6
-363.564685	7
-363.592326	8
-363.595614	9

(b) k-point Convergence

Table 6.5: Convergence values for Titanium

6.5 Total Energy Calculation for binary systems

6.5.1 Nickel-Titanium

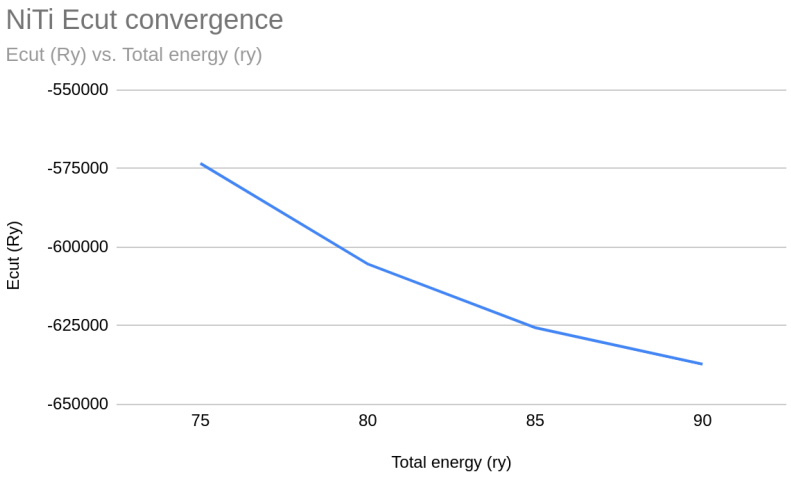

(a) E_{cut} Convergence

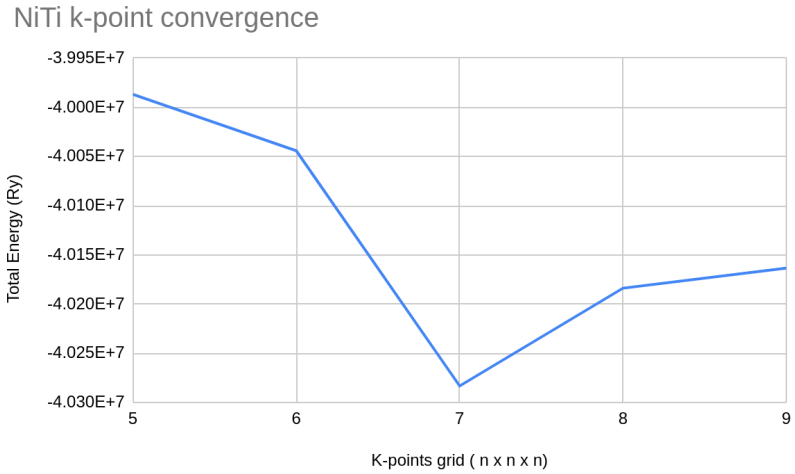

(b) k-point Convergence

Figure 6.4: Calculations for Ni-Ti

Total Energy	$E_{cut}(Ry)$
-608.573333	75
-608.605352	80
-608.625587	85
-608.637188	90

(a) E_{cut} Convergence

Total Energy	*k-points*
-608.39986814	5
-608.40044167	6
-608.40283246	7
-608.40183861	8
-608.40163384	9

(b) k-point Convergence

Table 6.6: Convergence values for Nickel - Titanium

6.5.2 Nickel-Zirconium

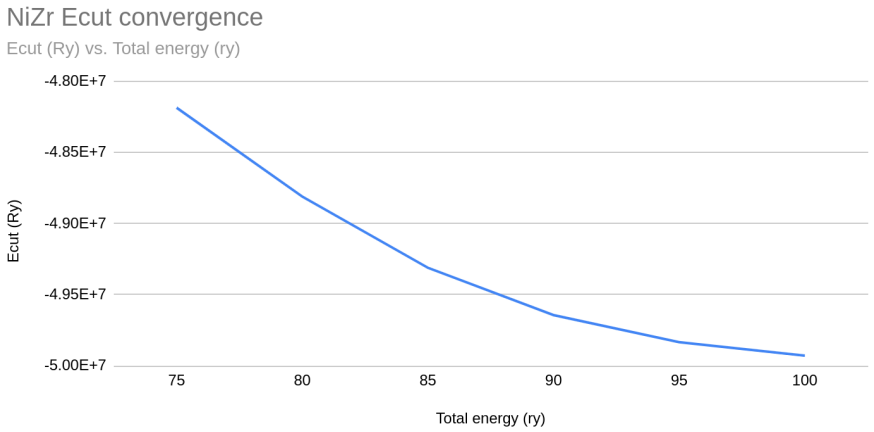

(a) E_{cut} Convergence

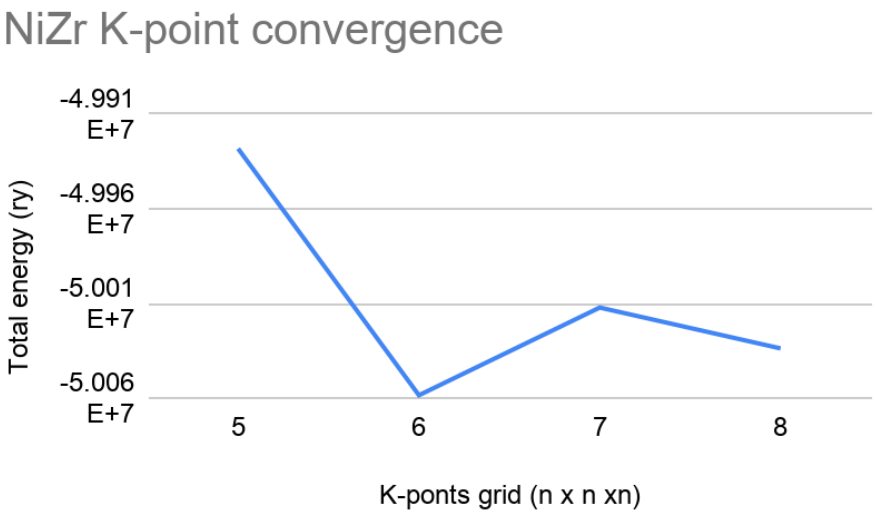

(b) k-point Convergence

Figure 6.5: Calculations for Ni-Zr

Total Energy	$E_{cut}(Ry)$
-1459.48186551	75
-1459.48811348	80
-1459.49311290	85
-1459.49643965	90
-1459.49834431	95
-1459.49928244	100

(a) E_{cut} Convergence

Total Energy	*k-points*
-499.28244	5
-500.58178	6
-500.11977	7
-500.33505	8

(b) k-point Convergence

Table 6.7: Convergence values for Nickel - Zirconium

Chapter 7

Conclusions and Future Work

From the critical review of Ni-Ti-Zr ternary system which includes the incorporation of all the recent developments, assessments and experimental data, we conclude that there exists a ternary phase which is present at temperatures >1300 °C along the composition of NiTi - NiZr binaries. There is insufficient data in the temperature range between 1200 - 1300 °C which needs to be explored for extrapolating the results further to higher temperature. This can be costly and difficult to perform experimentally. The critical assessment performed in this work will lay the foundation for further extrapolation of stability range of the ternary compound in the given temperature range. Also it will provide the solubility range of the compound.

Crystallographic information plays a vital for the property of materials. In the present work,

- The binary compound NiTi is in B2 crystal structure with 2 atoms in the primitive cell and NiZr in orthorhombic crystal structure with 4 atoms in the primitive cell.
- The required cut-off energy and k-point for geometric optimisation are calculated by series of single point energy calculation.
- The calculated energy of formation of standard reference state structure of NiTi and NiZr at 0K are comparable with literature data.

7.1 Suggestions for Future work

Further work is required to obtain more insight on the crystal structure of the ternary compound. DFT calculations are needed for the various ternary structures suggested by authors to calculate the one with minimum energy. The crystal structure will provide us with a better understanding of the physical properties of the compound as well as the solubility range in the other binaries.

Bibliography

[Becke, 1993] Becke, A. D. (1993). A new mixing of hartree–fock and local density-functional theories. *The Journal of chemical physics*, 98(2):1372–1377.

[Bellen et al., 1996] Bellen, P., Kumar, K. H., and Wollants, P. (1996). Thermodynamic assessment of the ni-ti phase diagram. *Zeitschrift fur metallkunde*, 87(12):972–978.

[Blöchl, 1994] Blöchl, P. E. (1994). Projector augmented-wave method. *Physical review B*, 50(24):17953.

[Born, 1927] Born, M. (1927). Born-oppenheimer approximation. *Ann. Phys*, 84:457–484.

[Burke et al., 1998] Burke, K., Perdew, J. P., and Wang, Y. (1998). Derivation of a generalized gradient approximation: The pw91 density functional. In *Electronic density functional theory*, pages 81–111. Springer.

[Colinet et al., 1985] Colinet, C., Pasturel, A., and Hicter, P. (1985). Trends in cohesive energy of transition metal alloys. *Calphad*, 9(1):71–99.

[Gachon et al., 1981] Gachon, J., Notin, M., and Hertz, J. (1981). The enthalphy of mixing of the intermediate phases in the systems feti, coti, and niti by direct reaction calorimetry. *Thermochimica Acta*, 48(1-2):155–164.

[Guo and Kleppa, 1998] Guo, Q. and Kleppa, O. (1998). Standard enthalpies of formation of some alloys formed between group iv elements and group viii elements, determined by high-temperature direct synthesis calorimetry: I. alloys of (ti, zr, hf) with (rh, pd, pt). *Journal of alloys and compounds*, 266(1-2):224–229.

[Gupta, 1999] Gupta, K. (1999). The ni-ti-zr system (nickel-titanium-zirconium). *Journal of phase equilibria*, 20(4):441.

[Haiyan and Zhanpeng, 1993] Haiyan, L. and Zhanpeng, J. (1993). A reassessment of the ti ni system. *Calphad*, 17(4):415–426.

[Henaff et al., 1984] Henaff, M., Colinet, C., Pasturel, A., and Buschow, K. (1984). Study of the enthalpies of formation and crystallization in the system zr-ni. *Journal of applied physics*, 56(2):307–310.

[Hennig et al., 2005] Hennig, R., Carlsson, A., Kelton, K., and Henley, C. (2005). Ab initio ti-zr-ni phase diagram predicts stability of icosahedral tizrni quasicrystals. *Physical Review B*, 71(14):144103.

[Hohenberg and Kohn, 1964] Hohenberg, P. and Kohn, W. (1964). Inhomogeneous electron gas. *Physical review*, 136(3B):B864.

[Jana et al., 2020] Jana, A., Sridar, S., Fries, S. G., Hammerschmidt, T., and Kumar, K. H. (2020). Thermodynamic modelling of the ni–zr system. *Intermetallics*, 116:106640.

[Jia et al., 1994] Jia, C., Ishida, K., and Nishizawa, T. (1994). Experimental methods of phase diagram determination, ed. by je morral. *RS Schiffman and SM Merchant, The Mineral and Materials Society, Warrandale, USA*, page 31.

[Kauffman and Mayo, 1997] Kauffman, G. B. and Mayo, I. (1997). The story of nitinol: the serendipitous discovery of the memory metal and its applications. *The chemical educator*, 2(2):1–21.

[Kaufman and Nesor, 1978] Kaufman, L. and Nesor, H. (1978). Coupled phase diagrams and thermochemical data for transition metal binary systems—ii. *Calphad*, 2(1):81–108.

[Khan et al., 2017] Khan, A. N., Muhyuddin, M., and Wadood, A. (2017). Development and characterization of nickel–titanium–zirconium shape memory alloy for engineering applications. *Russian Journal of Non-Ferrous Metals*, 58(5):509–515.

[Kirklin et al., 2015] Kirklin, S., Saal, J. E., Meredig, B., Thompson, A., Doak, J. W., Aykol, M., Rühl, S., and Wolverton, C. (2015). The open quantum materials database (oqmd): assessing the accuracy of dft formation energies. *npj Computational Materials*, 1(1):1–15.

[Kohn, 1986] Kohn, W. (1986). Density-functional theory for excited states in a quasi-local-density approximation. *Physical Review A*, 34(2):737.

[Kohn and Sham, 1965] Kohn, W. and Sham, L. J. (1965). Self-consistent equations including exchange and correlation effects. *Physical review*, 140(4A):A1133.

[Kresse and Joubert, 1999] Kresse, G. and Joubert, D. (1999). From ultrasoft pseudopotentials to the projector augmented-wave method. *Physical review b*, 59(3):1758.

[Kubaschewski, 1956] Kubaschewski, O. (1956). H. villa u. wa dench. *Trans. Faraday Soc*, 52:214.

[Liu et al., 2015] Liu, X., Huang, L., Yang, S., Huang, Y., Zhang, J., Li, J., Zhu, J., Jiang, H., and Wang, C. (2015). Experimental investigation of isothermal sections (1000, 1200 c) in the ni-ti-zr system. *Journal of Phase Equilibria and Diffusion*, 36(5):414–421.

[Miedema, 1973] Miedema, A. (1973). Simple model for alloys. *Philips Tech. Rev*, 33:149–160.

[Monkhorst and Pack, 1976] Monkhorst, H. J. and Pack, J. D. (1976). Special points for brillouin-zone integrations. *Physical review B*, 13(12):5188.

[Murray, 1987] Murray, J. L. (1987). Phase diagrams of binary titanium alloys. *ASM international*, pages 340–345.

[Nash, 1991] Nash, P. (1991). Phase diagrams of binary nickel alloys. *ASM International(USA), 1991,*, page 394.

[Pasturel et al., 1995] Pasturel, A., Colinet, C., Manh, D. N., Paxton, A., and Van Schilfgaarde, M. (1995). Electronic structure and phase stability study in the ni-ti system. *Physical Review B*, 52(21):15176.

[Perdew et al., 1996] Perdew, J. P., Burke, K., and Wang, Y. (1996). Generalized gradient approximation for the exchange-correlation hole of a many-electron system. *Physical Review B*, 54(23):16533.

[Perdew and Levy, 1983] Perdew, J. P. and Levy, M. (1983). Physical content of the exact kohn-sham orbital energies: band gaps and derivative discontinuities. *Physical Review Letters*, 51(20):1884.

[Perdew and Schmidt, 2001] Perdew, J. P. and Schmidt, K. (2001). Jacob's ladder of density functional approximations for the exchange-correlation energy. In *AIP Conference Proceedings*, volume 577, pages 1–20. American Institute of Physics.

[Phillips, 1958] Phillips, J. C. (1958). Energy-band interpolation scheme based on a pseudopotential. *Physical Review*, 112(3):685.

[Phillips and Kleinman, 1959] Phillips, J. C. and Kleinman, L. (1959). New method for calculating wave functions in crystals and molecules. *Physical Review*, 116(2):287.

[Santhy and Kumar, 2010] Santhy, K. and Kumar, K. H. (2010). Thermodynamic assessment of mo-ni-ti ternary system by coupling first-principle calculations with calphad approach. *Intermetallics*, 18(9):1713–1721.

[Saunders and Chandrasekaran, 1992] Saunders, N. and Chandrasekaran, L. (1992). Phase diagram modeling for titanium alloys with light element impurities. *Journal of Phase Equilibria*, 13(6):612–619.

[Sridar et al., 2017] Sridar, S., Kumar, R., and Kumar, K. H. (2017). Thermodynamic modelling of ti-zr-n system. *Calphad*, 56:102–107.

[Tang et al., 1999] Tang, W., Sundman, B., Sandström, R., and Qiu, C. (1999). New modelling of the b2 phase and its associated martensitic transformation in the ti–ni system. *Acta materialia*, 47(12):3457–3468.

[Thiedemann et al., 1999] Thiedemann, U., Rösner-Kuhn, M., Drewes, K., Kuppermann, G., and Frohberg, M. G. (1999). Mixing enthalpy measurements of liquid ti-zr, fe-ti-zr and fe-ni-zr alloys. *Steel research*, 70(1):3–8.

[Tokunaga et al., 2007] Tokunaga, T., Matsumoto, S., Ohtani, H., and Hasebe, M. (2007). Thermodynamic calculation of phase equilibria in the nb-ni-ti-zr quaternary system. *Materials transactions*, 48(2):89–96.

[Van Vucht, 1966] Van Vucht, J. (1966). Influence of radius ratio on the structure of intermetallic compounds of the ab3 type. *Journal of the Less Common Metals*, 11(5):308–322.

[Vanderbilt, 1990] Vanderbilt, D. (1990). Soft self-consistent pseudopotentials in a generalized eigenvalue formalism. *Physical review B*, 41(11):7892.

[Watson and Bennett, 1981] Watson, R. and Bennett, L. (1981). Optimized prediction for heats of formation of transition metal alloys. *Calphad*, 5(1):25–40.

[Yeh et al., 2014] Yeh, M.-C., Li, J. L., Lo, P. J., and Hsieh, K.-C. (2014). Phase equilibrium in the ni-ti-zr system at 800 c. *Journal of phase equilibria and diffusion*, 35(2):157–162.

[Yi and Moore, 1989] Yi, H. and Moore, J. (1989). Combustion synthesis of tini intermetallic compounds. *Journal of materials science*, 24(10):3456–3462.

[Zaitsev et al., 2002] Zaitsev, A., Zaitseva, N., Shakhpazov, E. K., and Kodentsov, A. A. (2002). Thermodynamic properties and phase equilibria in the nickel–zirconium system. the liquid to amorphous state transition. *Physical Chemistry Chemical Physics*, 4(24):6047–6058.

[Zhang et al., 2007] Zhang, R., Sheng, S., and Liu, B. (2007). Predicting the formation enthalpies of binary intermetallic compounds. *Chemical physics letters*, 442(4-6):511–514.